[Earth's Future]

Supporting Information for

Future global population exposure to record-breaking climate extremes

Bohao Li[1,2], Kai Liu[1,3,*], Ming Wang[1], Qianzhi Wang[1,4], Qian He[2], Chenxia Li[5]

[1] School of National Safety and Emergency Management, Beijing Normal University, Beijing 100875, China.

[2] Faculty of Geographical Science, Beijing Normal University, Beijing 100875, China.

[3] Collaborative Innovation Centre on Forecast and Evaluation of Meteorological Disasters (CIC-FEMD), Nanjing University of Information Science & Technology, Nanjing 210044, China

[4] School of Systems Science, Beijing Normal University, Beijing 100875, China.

[5] College of Resources, Environment and Tourism, Capital Normal University, Beijing 100048, China

*Corresponding author: Kai Liu (liukai@bnu.edu.cn)

Contents of this file

Introduction

Figures and tables explain some of the information mentioned in the article; all figures and tables are referenced in the main text.

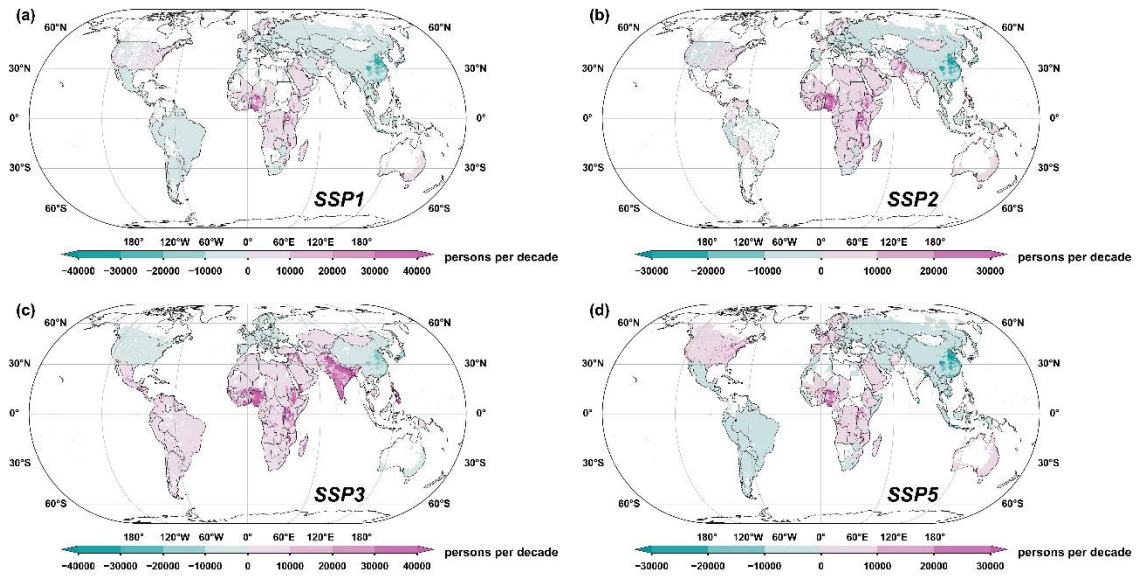

Figure S1. Population trends from 2020 to 2090 based on decadal linear regression at the 0.05 significance level: (a) SSP1, (b) SSP2, (c) SSP3, and (d) SSP5.

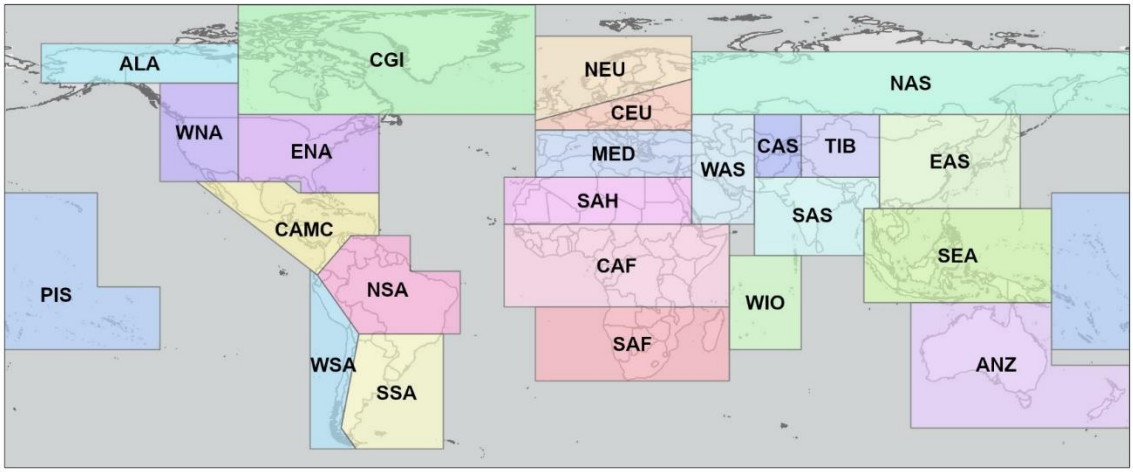

ALA	Alaska/N.W. Canada	ENA	East North America	SAS	South Asia
ANZ	Australia/New Zealand	MED	South Europe/Mediterranean	SEA	Southeast Asia
CAF	Central Africa	NAS	North Asia	SSA	Southeastern South America
CAMC	Central America/Mexico/Caribbean	NEU	North Europe	TIB	Tibetan Plateau
CAS	Central Asia	NSA	Northern South America	WAS	West Asia
CEU	Central Europe	PIS	Pacific Islands	WIO	West Indian Ocean
CGI	Canada/Greenland/Iceland	SAF	Southern Africa	WNA	West North America
EAS	East Asia	SAH	Sahara	WSA	West Coast South America

Figure S2. Climate reference regions used in this study.

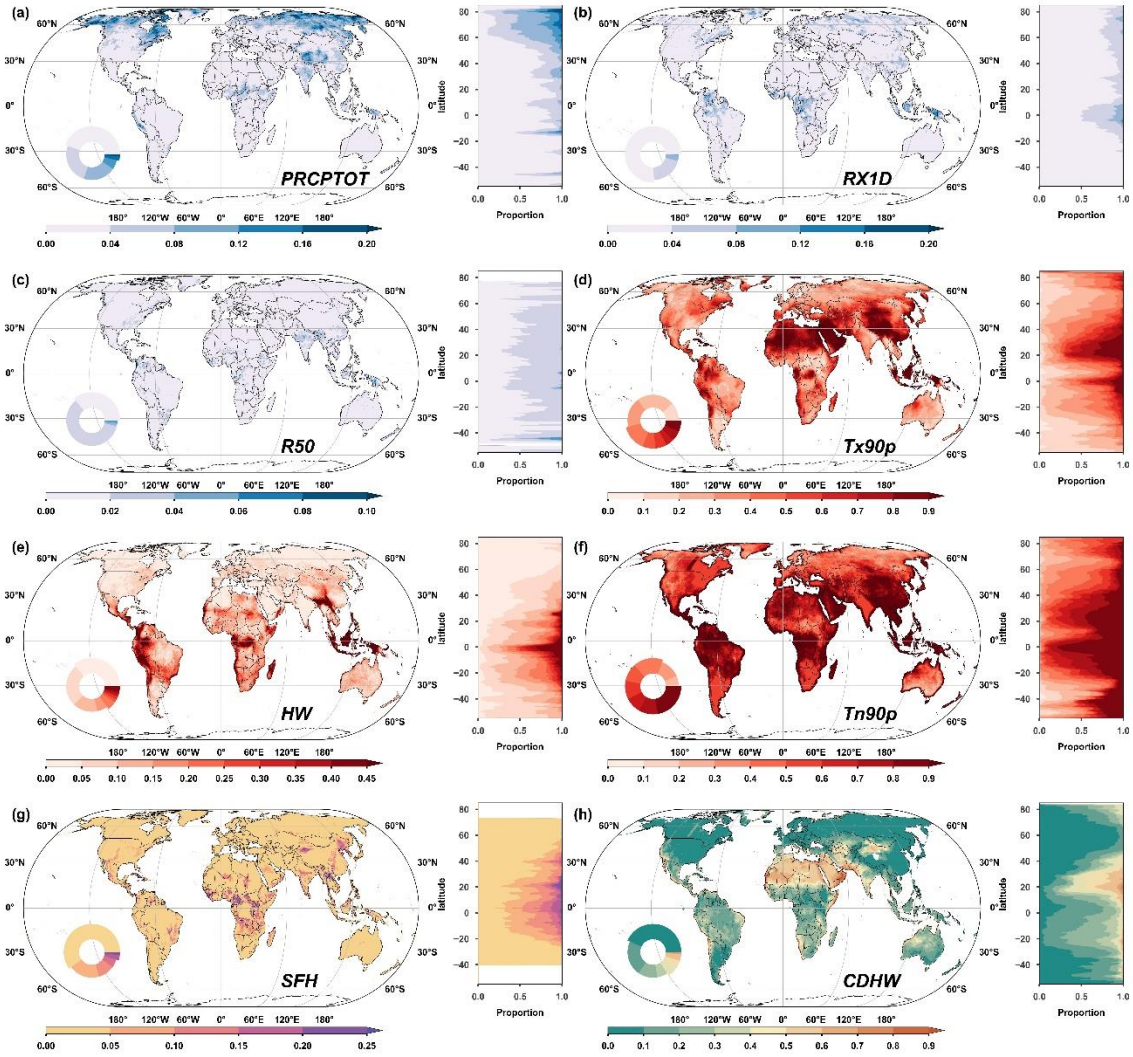

Figure S3. Annual record-breaking probability projections of multimodel medians for different climate extreme indices in the SSP1-2.6 scenario for the late-21st century: (a) PRCPTOT, (b) RX1D, (c) R50, (d) Tx90p, (e) HW, (f) Tn90p, (g) SFH, and (h) CDHW. The rings show the percentages of pixels at different record-breaking probability levels; the stacked charts demonstrate the proportions of record-breaking probability at each level at different latitudes.

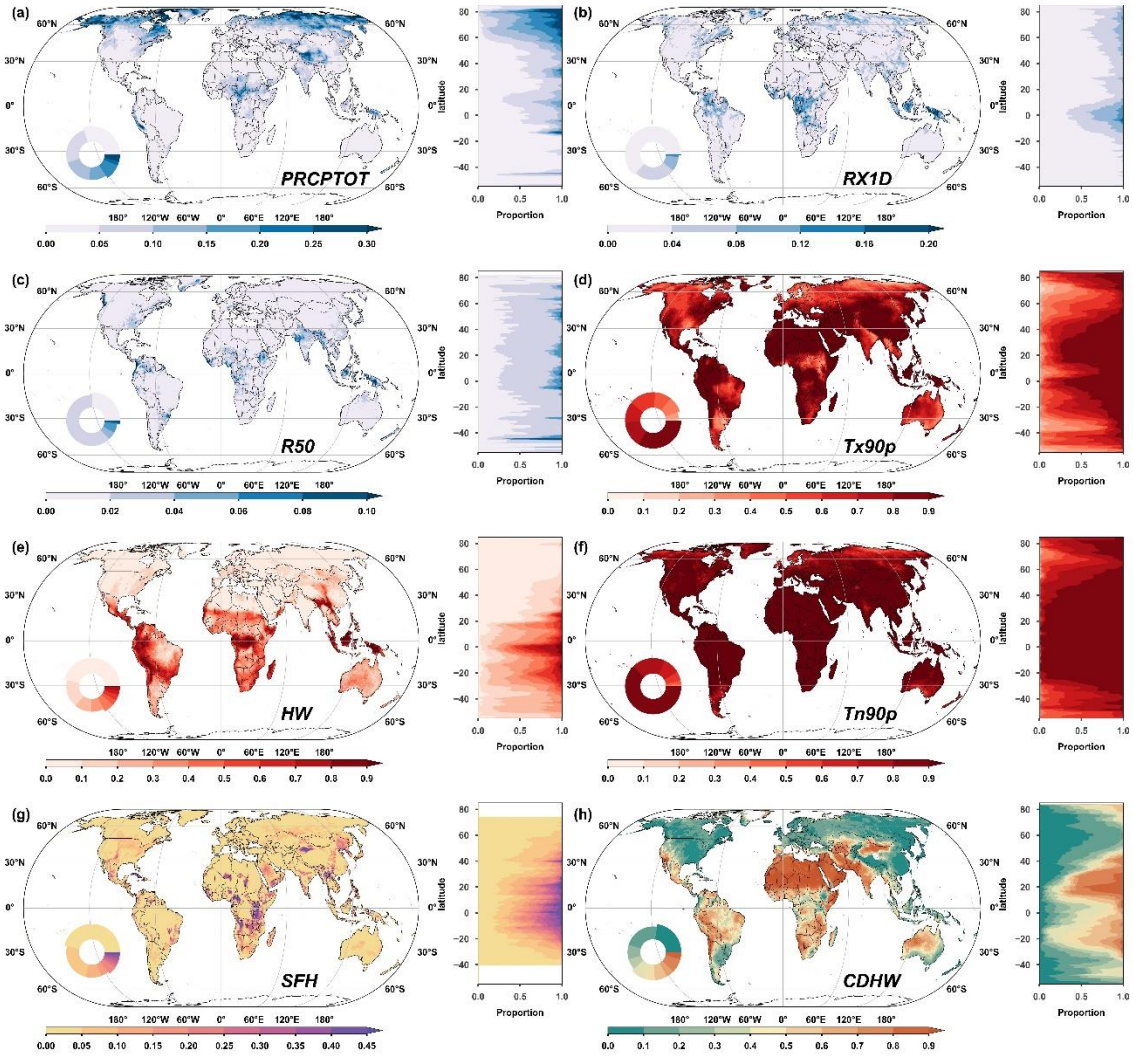

Figure S4. Annual record-breaking probability projections of multimodel medians for different climate extreme indices in the SSP2-4.5 scenario for the late-21st century: (a) PRCPTOT, (b) RX1D, (c) R50, (d) Tx90p, (e) HW, (f) Tn90p, (g) SFH, and (h) CDHW.

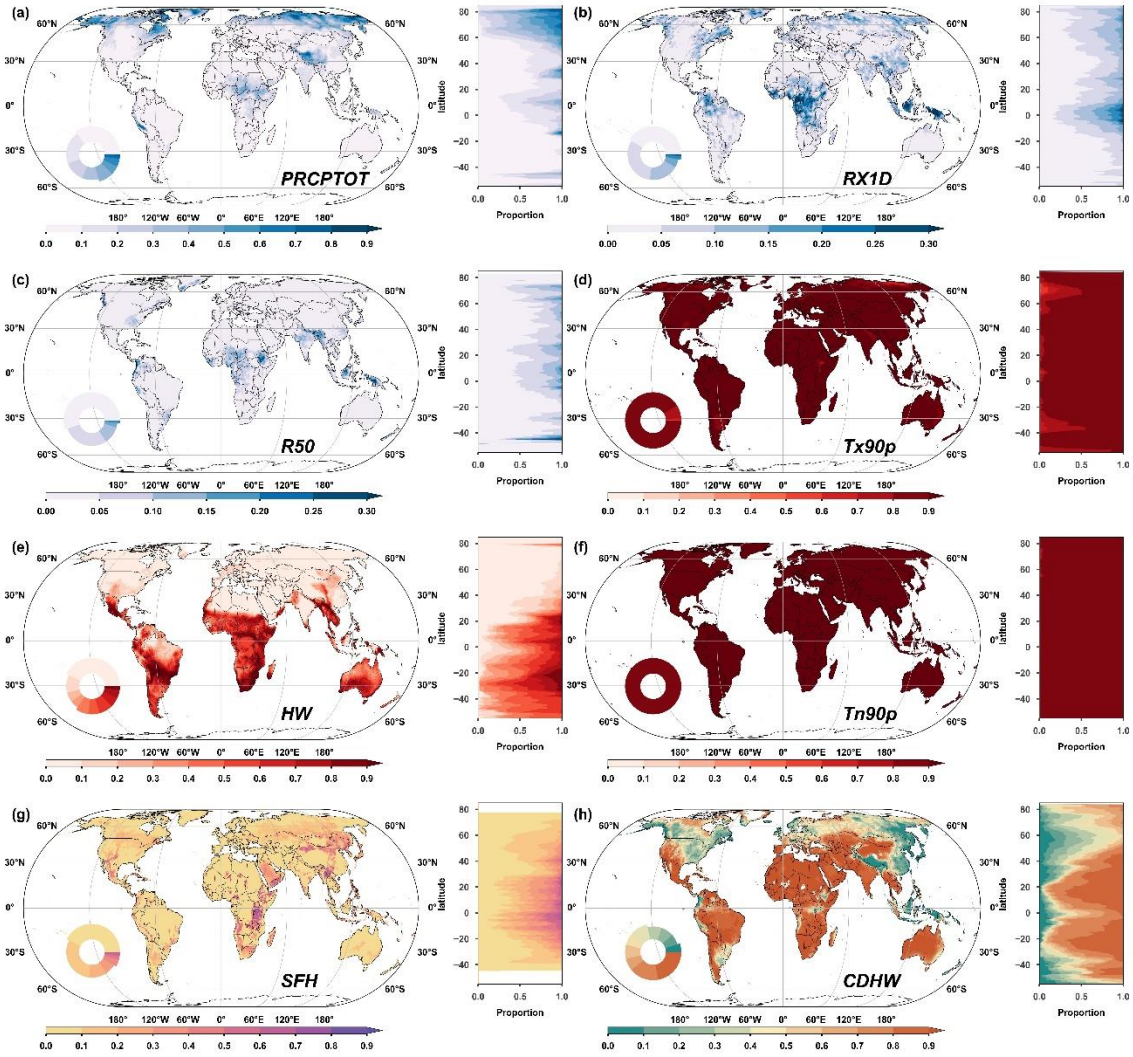

Figure S5. Annual record-breaking probability projections of multimodel medians for different climate extreme indices in the SSP5-8.5 scenario for the late-21st century: (a) PRCPTOT, (b) RX1D, (c) R50, (d) Tx90p, (e) HW, (f) Tn90p, (g) SFH, and (h) CDHW.

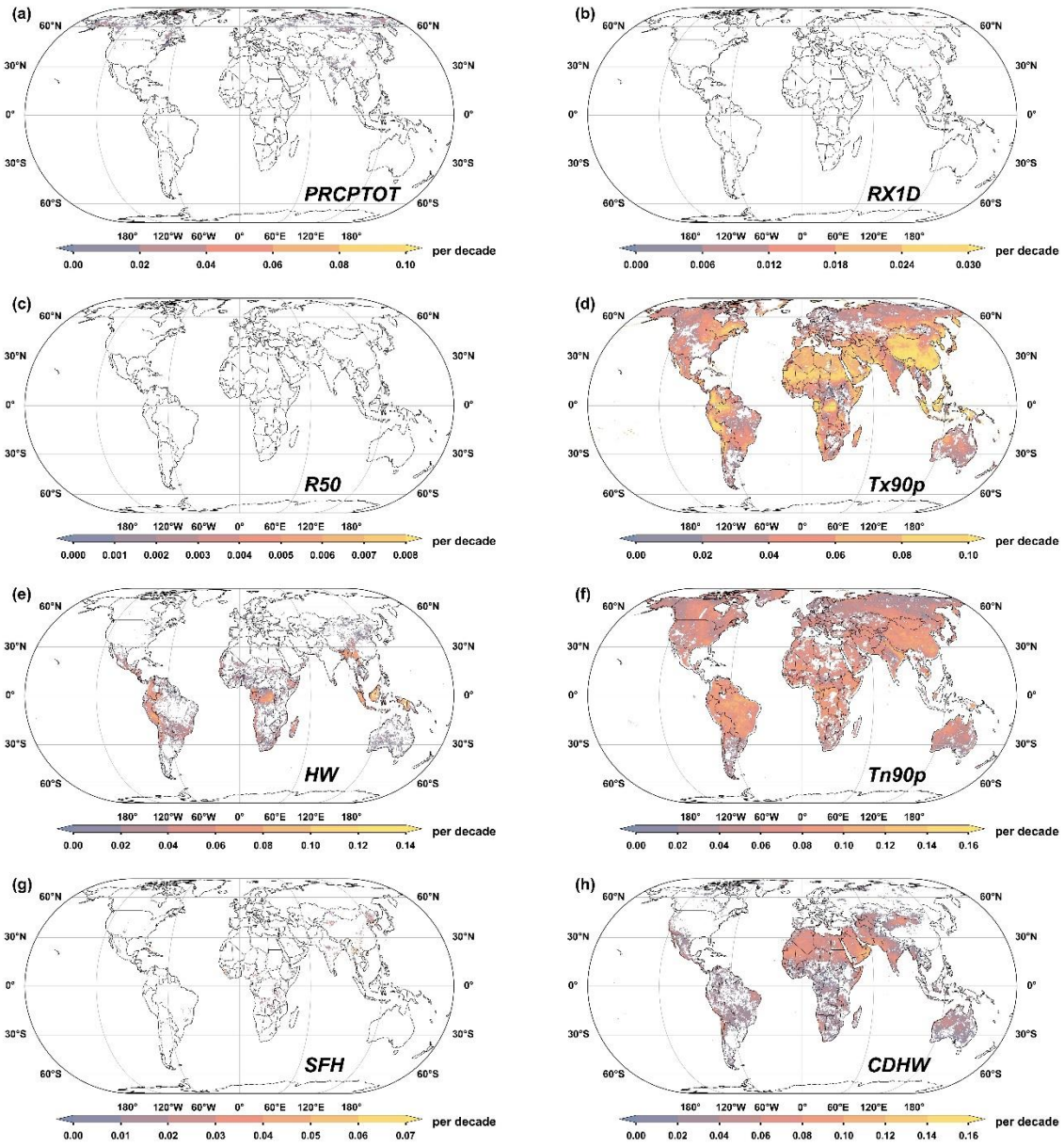

Figure S6. Trends in multimodel median record-breaking probabilities for different indices from the 2020s to 2090s based on decadal linear regression at the 0.05 significance level in the SSP1-2.6 scenario: (a) PRCPTOT, (b) RX1D, (c) R50, (d) Tx90p, (e) HW, (f) Tn90p, (g) SFH, and (h) CDHW.

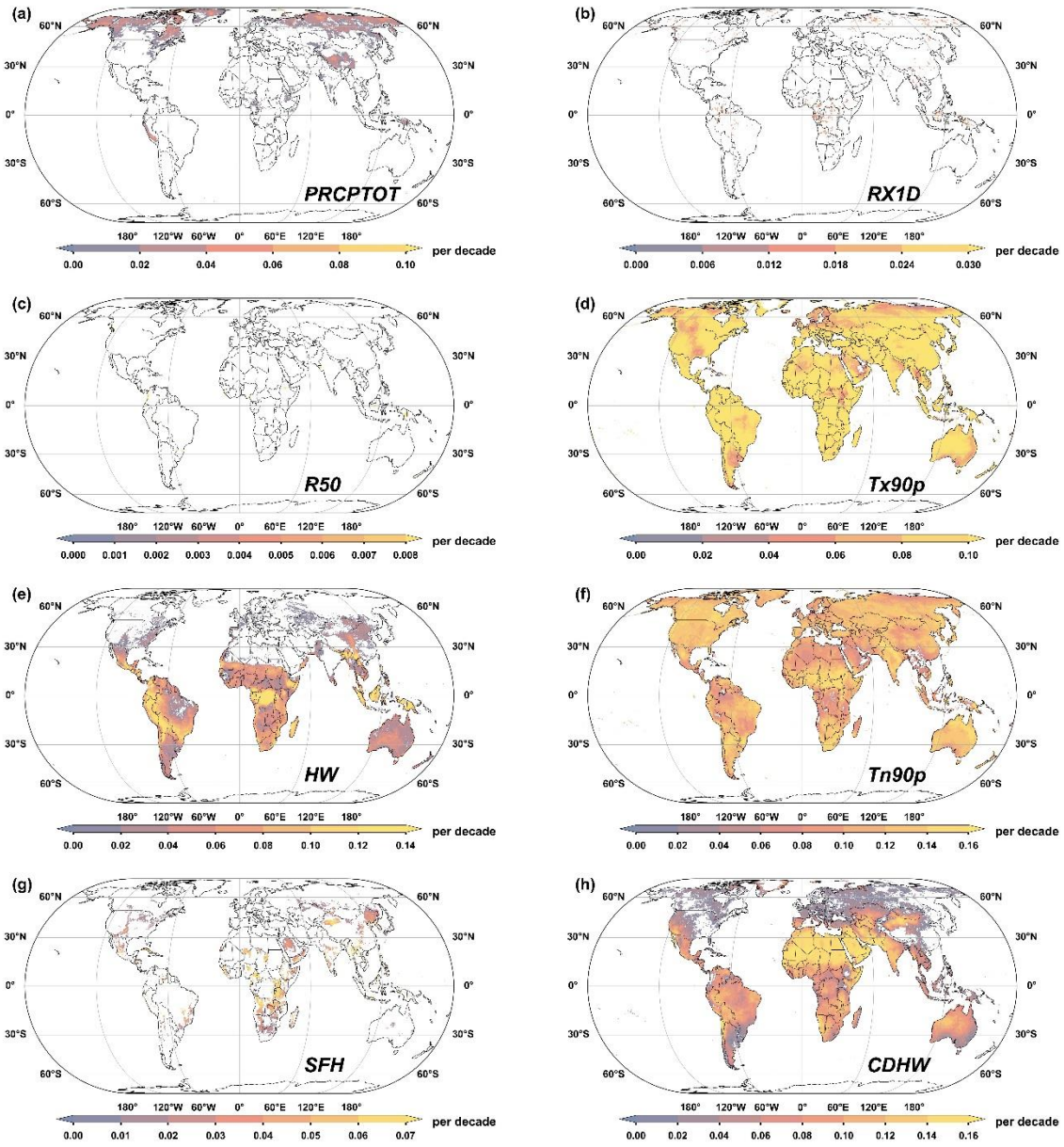

Figure S7. Trends in multimodel median record-breaking probabilities for different indices from the 2020s to 2090s based on decadal linear regression at the 0.05 significance level in the SSP2-4.5 scenario: (a) PRCPTOT, (b) RX1D, (c) R50, (d) Tx90p, (e) HW, (f) Tn90p, (g) SFH, and (h) CDHW.

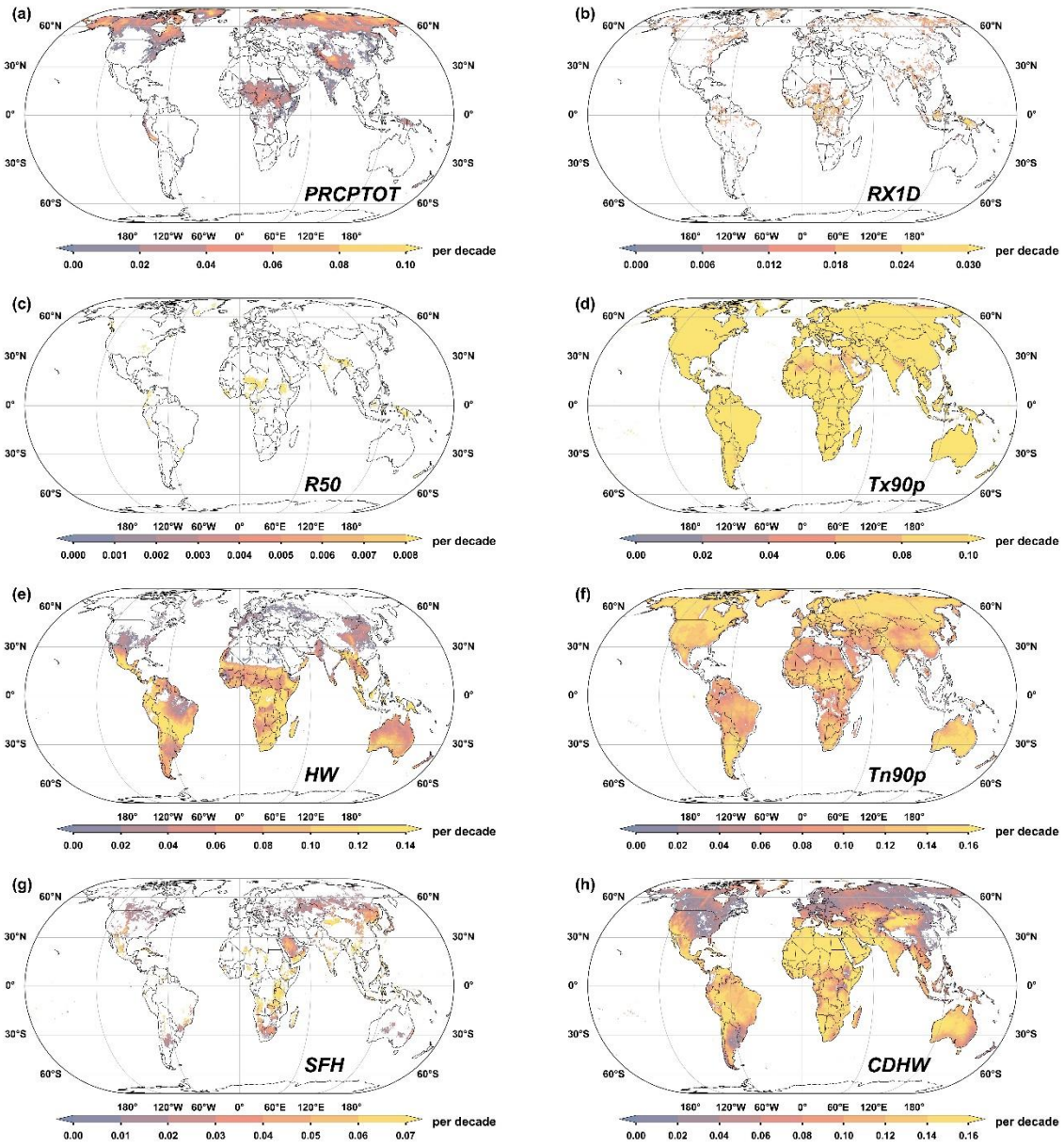

Figure S8. Trends in multimodel median record-breaking probabilities for different indices from the 2020s to 2090s based on decadal linear regression at the 0.05 significance level in the SSP3-7.0 scenario: (a) PRCPTOT, (b) RX1D, (c) R50, (d) Tx90p, (e) HW, (f) Tn90p, (g) SFH, and (h) CDHW.

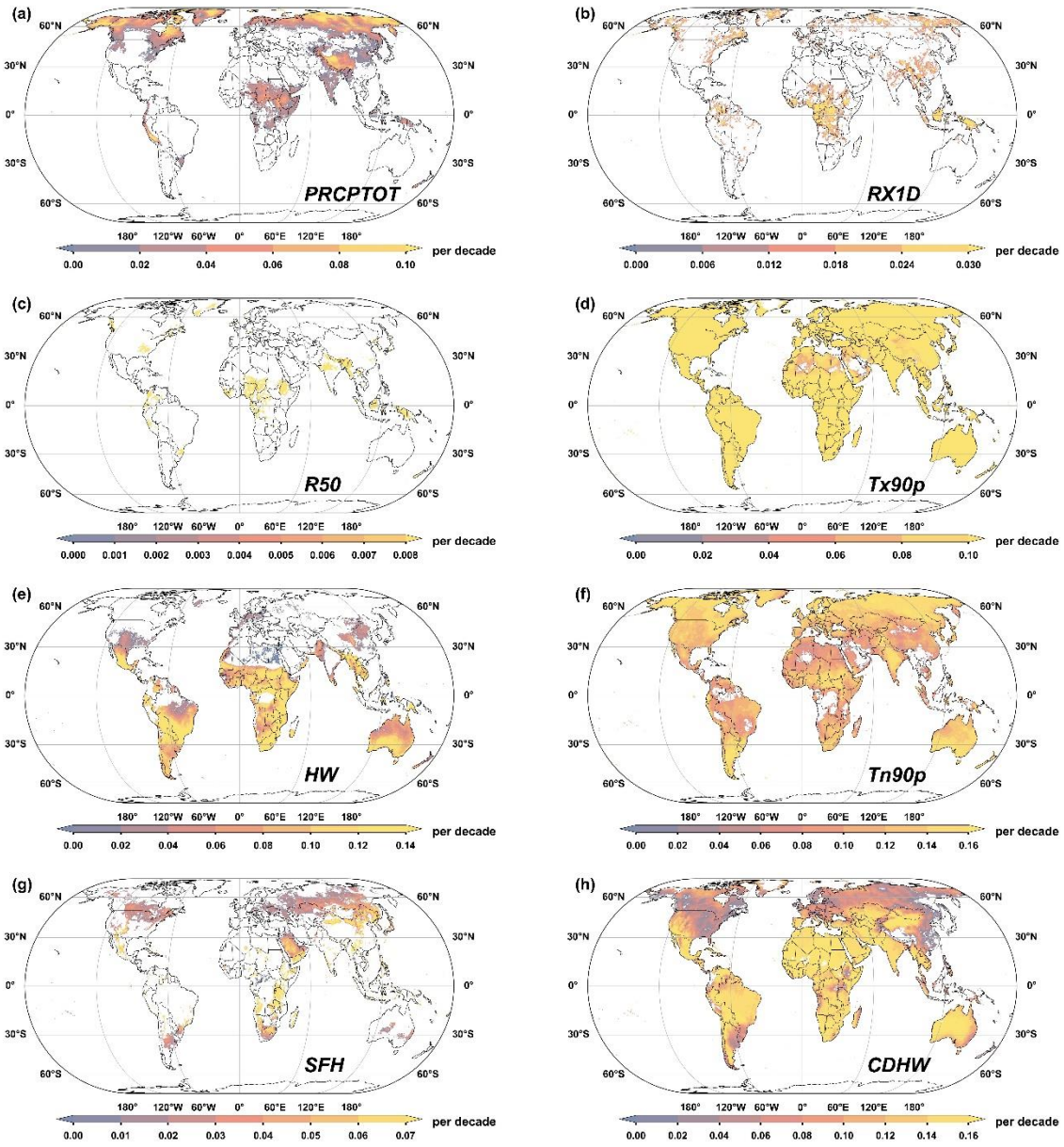

Figure S9. Trends in multimodel median record-breaking probabilities for different indices from the 2020s to 2090s based on decadal linear regression at the 0.05 significance level in the SSP5-8.5 scenario: (a) PRCPTOT, (b) RX1D, (c) R50, (d) Tx90p, (e) HW, (f) Tn90p, (g) SFH, and (h) CDHW.

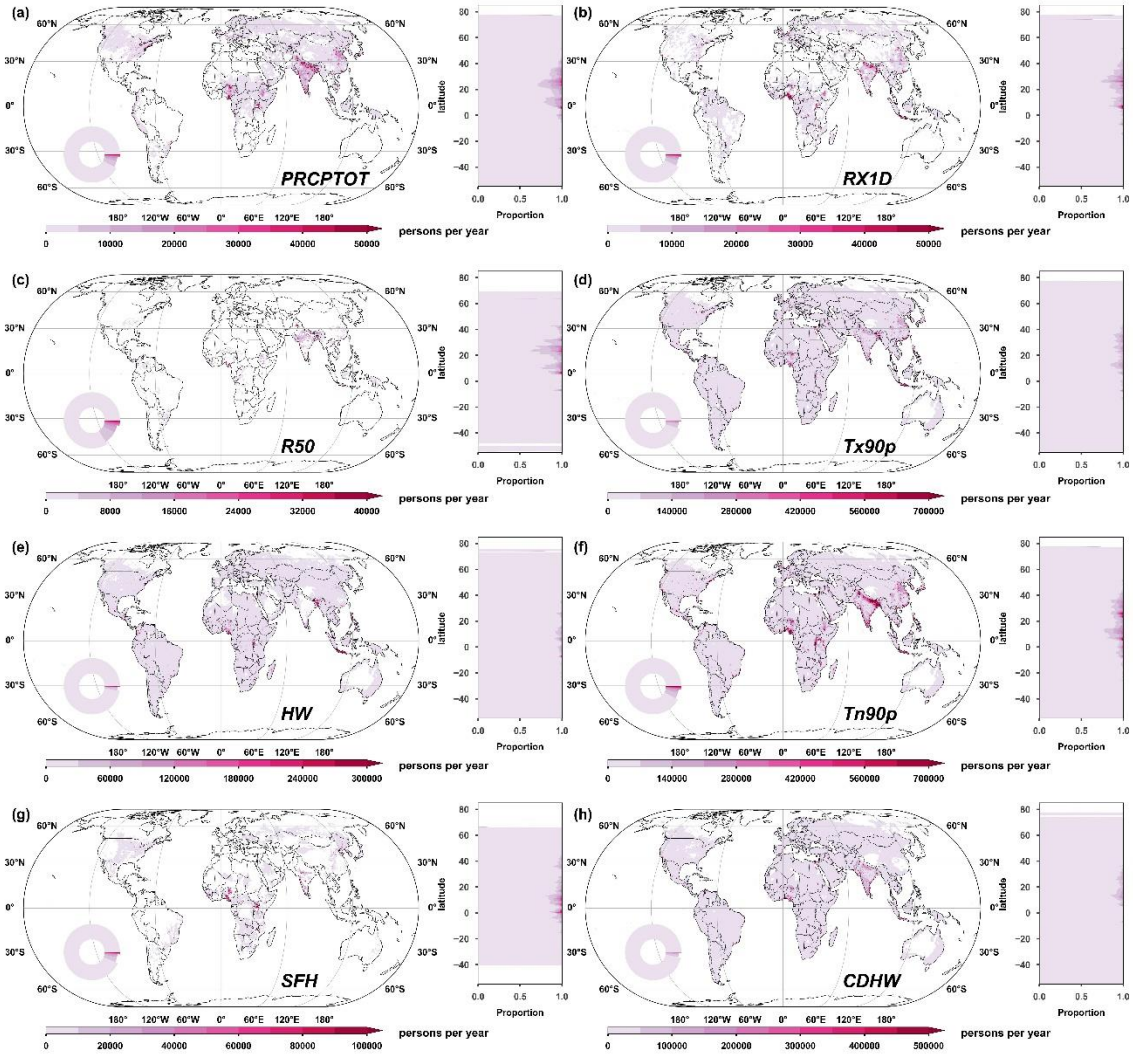

Figure S10. EAE projections of multimodel medians for different climate extreme indices in the SSP1-2.6 scenario for the late-21st century: (a) PRCPTOT, (b) RX1D, (c) R50, (d) Tx90p, (e) HW, (f) Tn90p, (g) SFH, and (h) CDHW. The rings show the percentages of pixels at different population exposure levels; the stacked charts demonstrate the proportions of population exposure at each level at different latitudes.

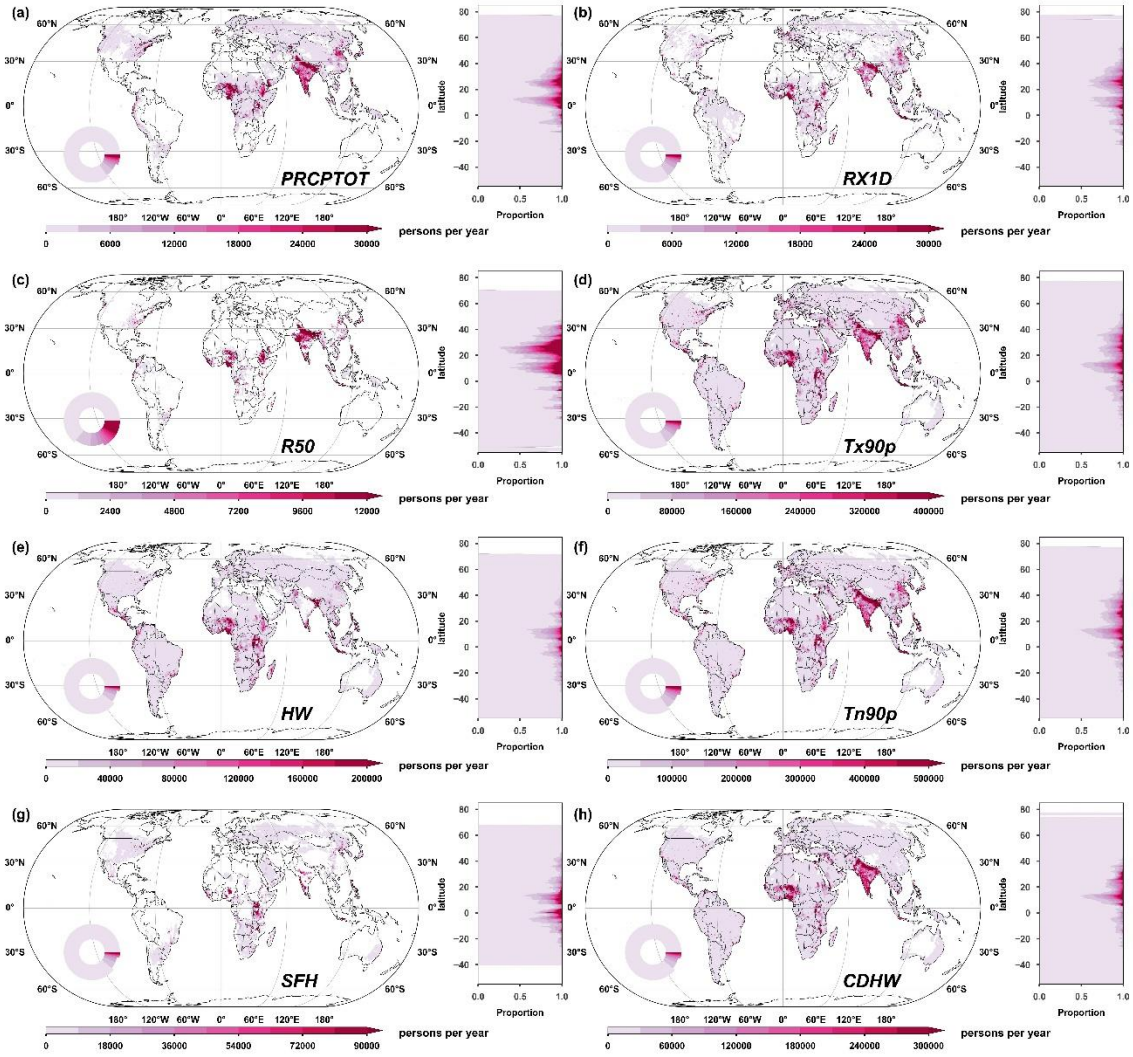

Figure S11. EAE projections of multimodel medians for different climate extreme indices in the SSP2-4.5 scenario for the late-21st century: (a) PRCPTOT, (b) RX1D, (c) R50, (d) Tx90p, (e) HW, (f) Tn90p, (g) SFH, and (h) CDHW.

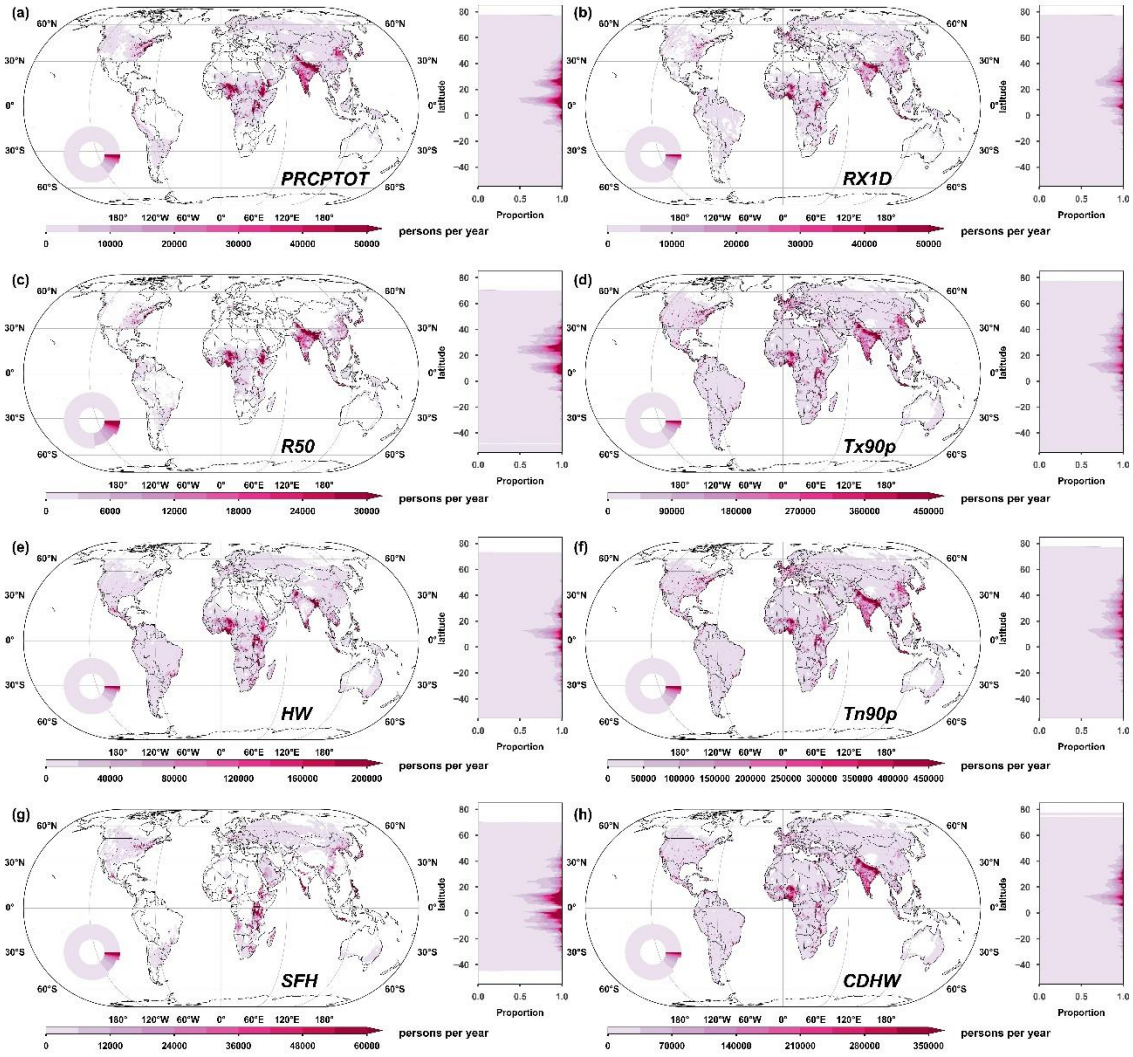

Figure S12. EAE projections of multimodel medians for different climate extreme indices in the SSP5-8.5 scenario for the late-21st century: (a) PRCPTOT, (b) RX1D, (c) R50, (d) Tx90p, (e) HW, (f) Tn90p, (g) SFH, and (h) CDHW.

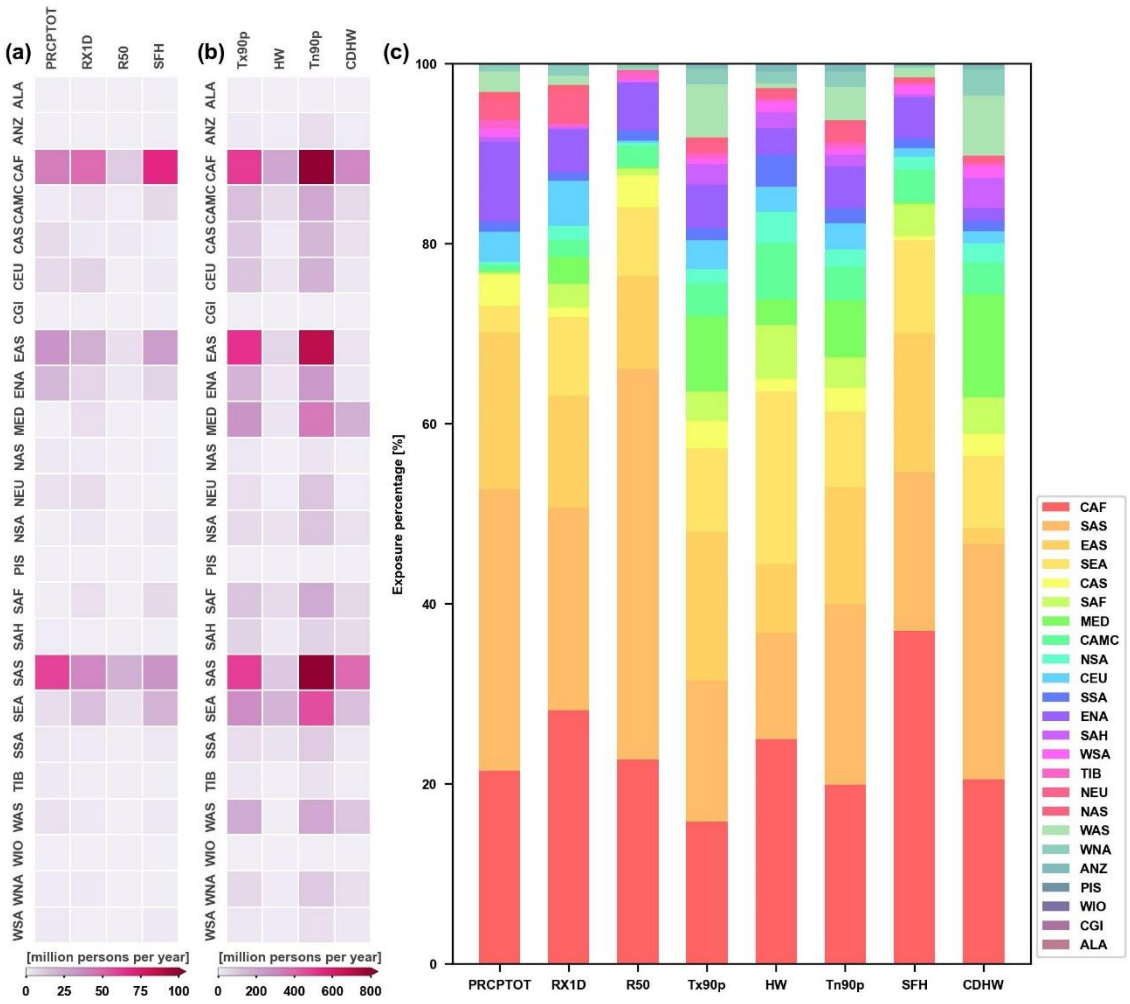

Figure S13. Subcontinental EAE projections of multimodel medians for different climate extreme indices in the SSP1-2.6 scenario for the late-21st century: (a) PRCPTOT, RX1D, R50, and SFH, (b) Tx90p, HW, Tn90p, and CDHW, and (c) regional percentage of the total global EAE.

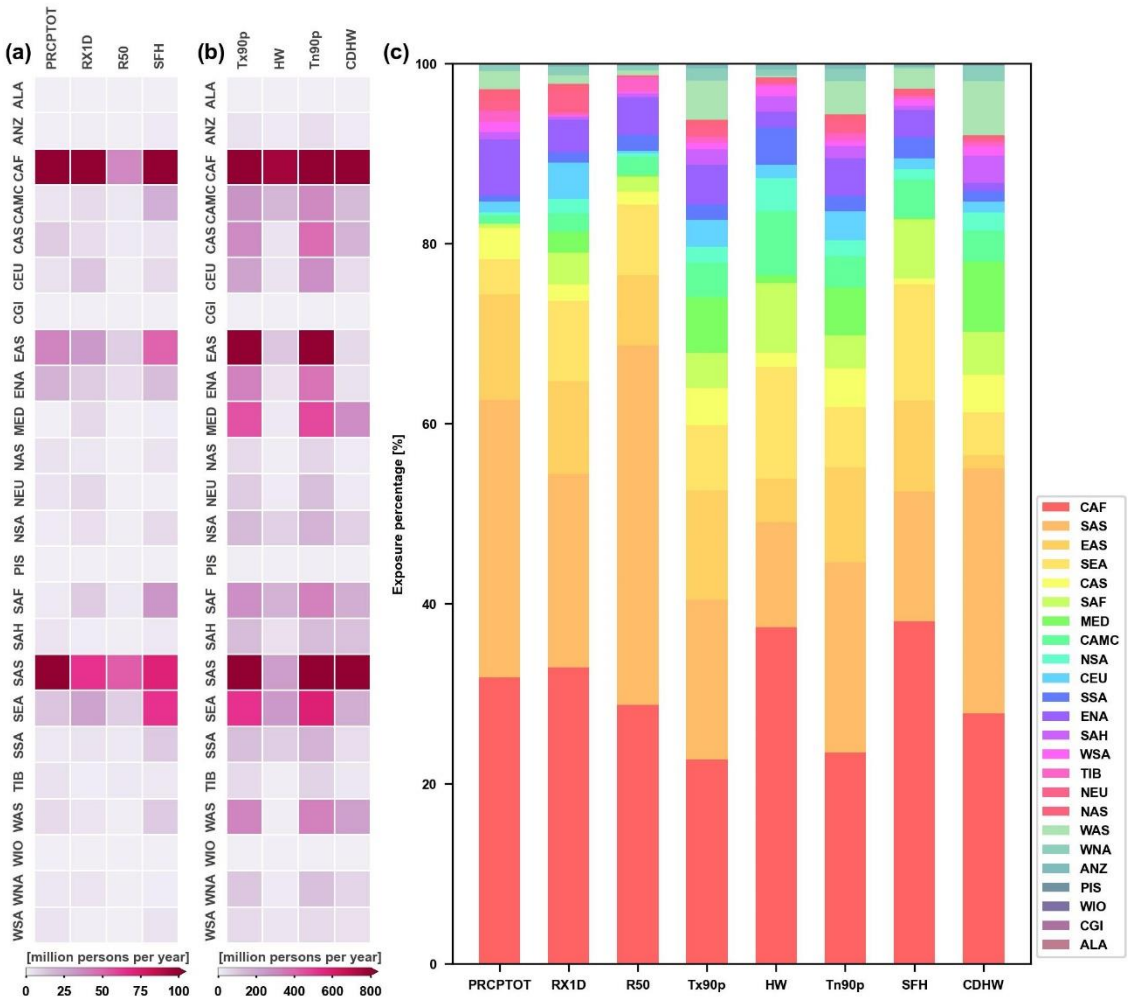

Figure S14. Subcontinental EAE projections of multimodel medians for different climate extreme indices in the SSP2-4.5 scenario for the late-21st century: (a) PRCPTOT, RX1D, R50, and SFH, (b) Tx90p, HW, Tn90p, and CDHW, and (c) regional percentage of the total global EAE.

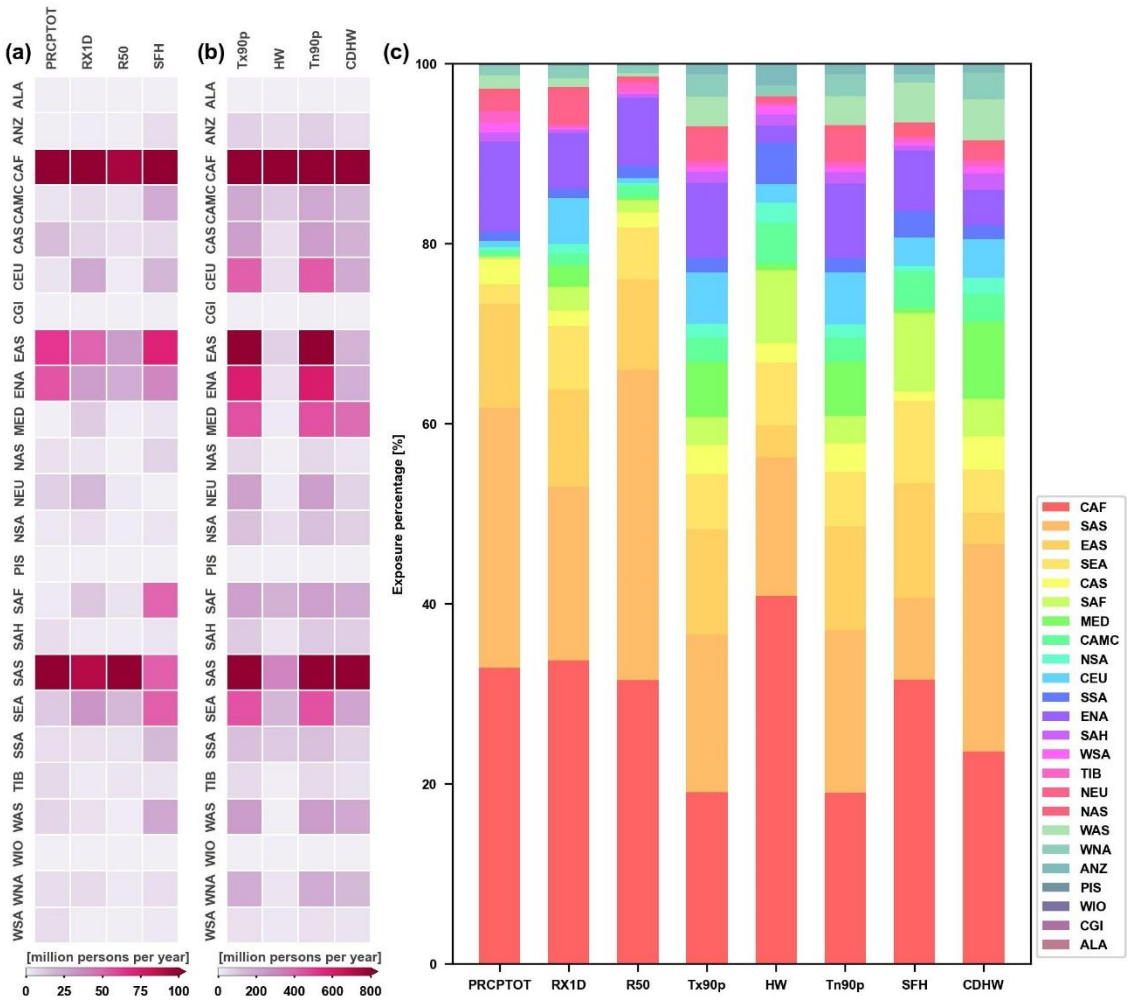

Figure S15. Subcontinental EAE projections of multimodel medians for different climate extreme indices in the SSP5-8.5 scenario for the late-21st century: (a) PRCPTOT, RX1D, R50, and SFH, (b) Tx90p, HW, Tn90p, and CDHW, and (c) regional percentage of the total global EAE.

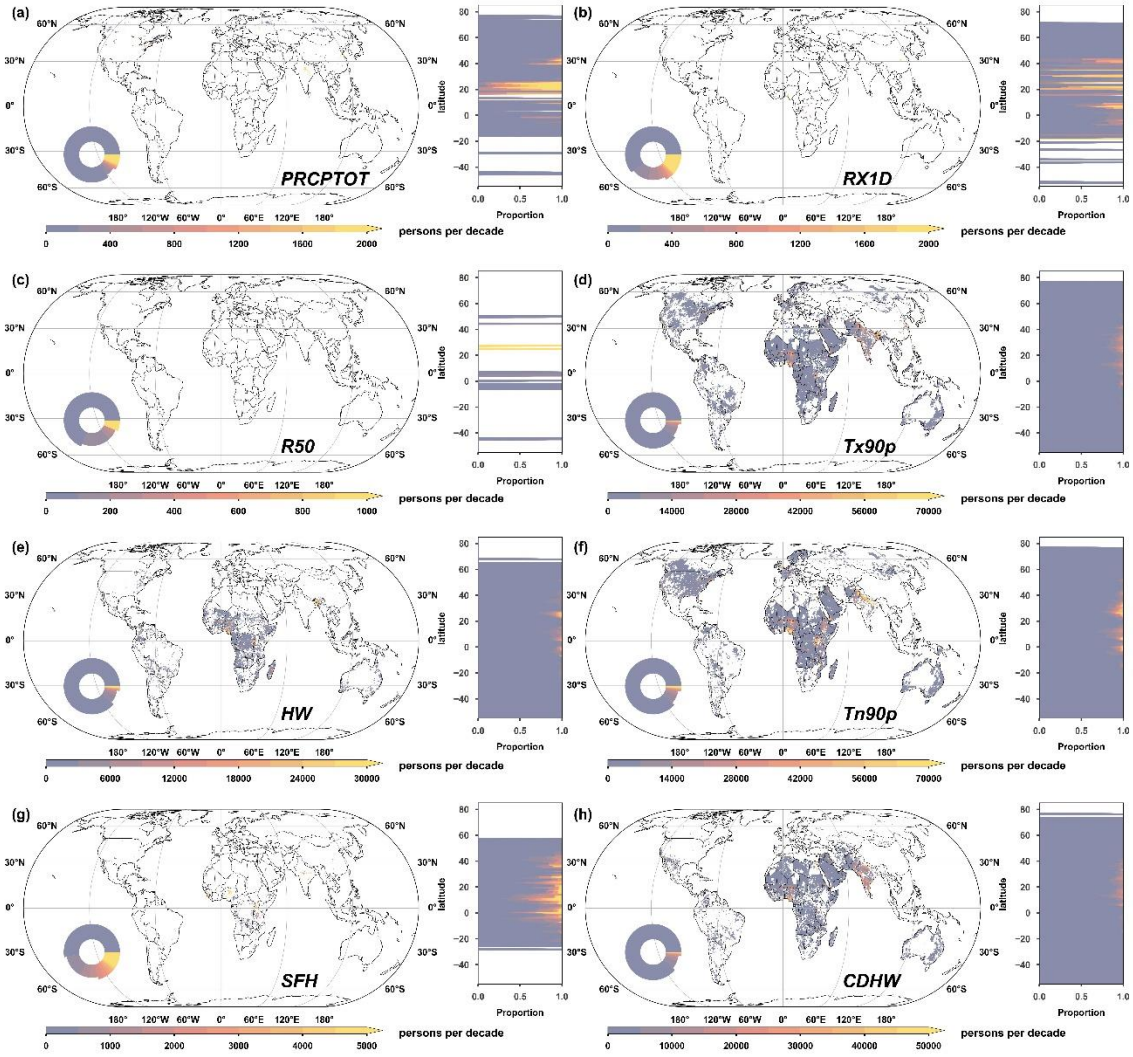

Figure S16. Multimodel median EAE growth rates for different climate extreme indices projected under the SSP1-2.6 scenario from the 2020s to 2090s: (a) PRCPTOT, (b) RX1D, (c) R50, (d) Tx90p, (e) HW, (f) Tn90p, (g) SFH, and (h) CDHW. The rings show the percentage of pixels at different EAE trend levels; the stacked charts demonstrate the percentage of EAE growth rates at each level at different latitudes.

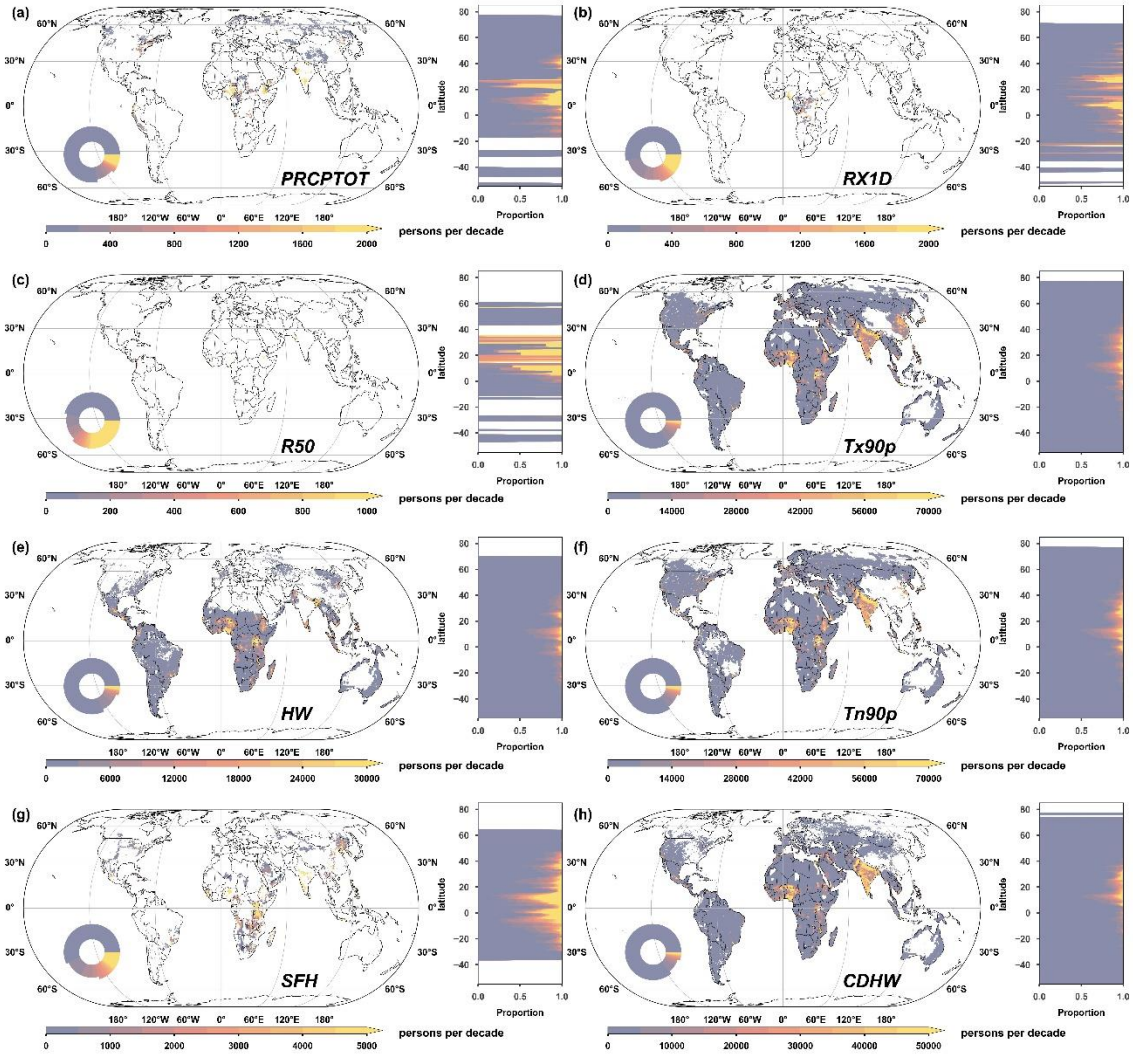

Figure S17. Multimodel median EAE growth rates for different climate extreme indices projected under the SSP2-4.5 scenario from the 2020s to 2090s: (a) PRCPTOT, (b) RX1D, (c) R50, (d) Tx90p, (e) HW, (f) Tn90p, (g) SFH, and (h) CDHW.

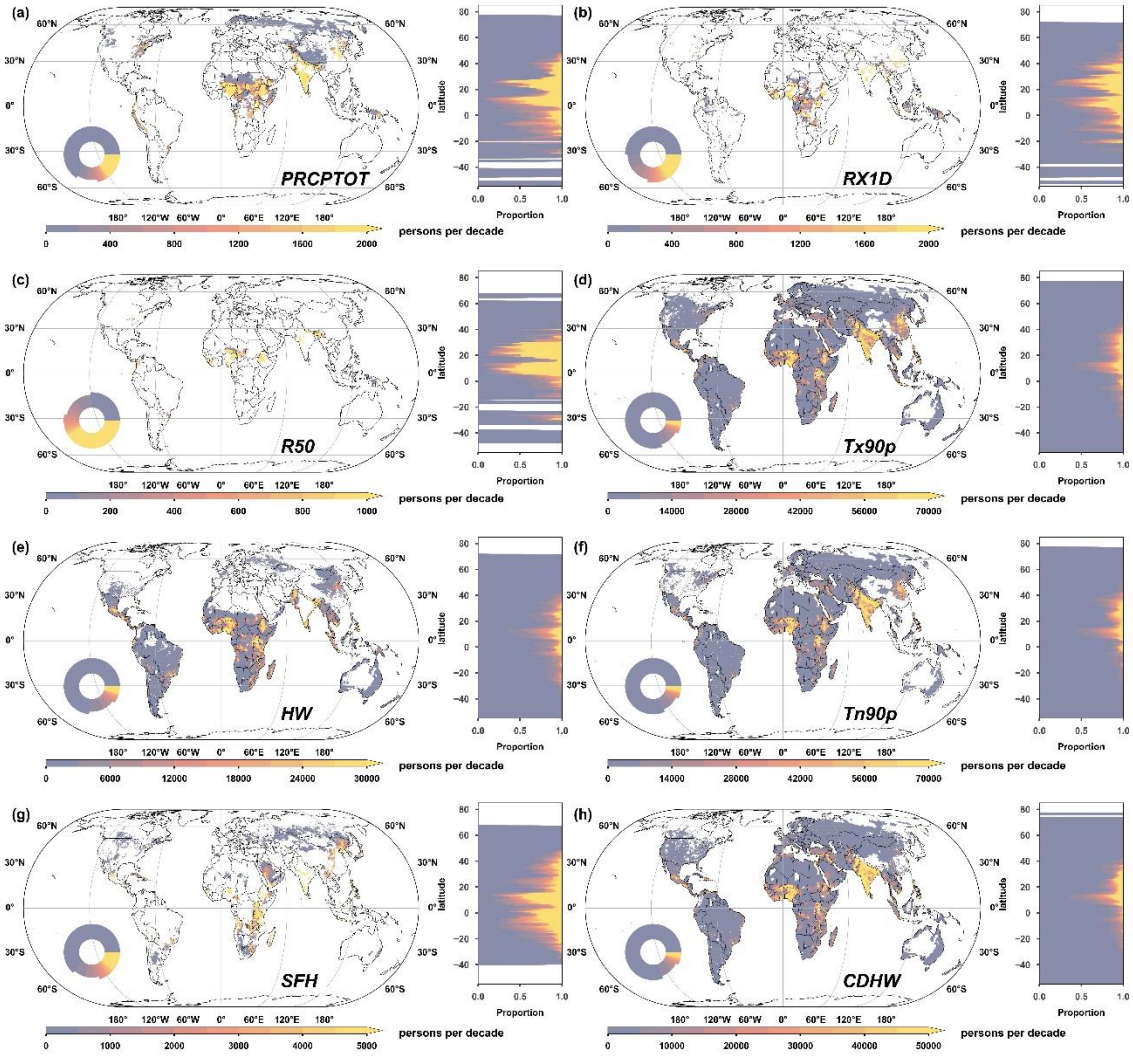

Figure S18. Multimodel median EAE growth rates for different climate extreme indices projected under the SSP3-7.0 scenario from the 2020s to 2090s: (a) PRCPTOT, (b) RX1D, (c) R50, (d) Tx90p, (e) HW, (f) Tn90p, (g) SFH, and (h) CDHW.

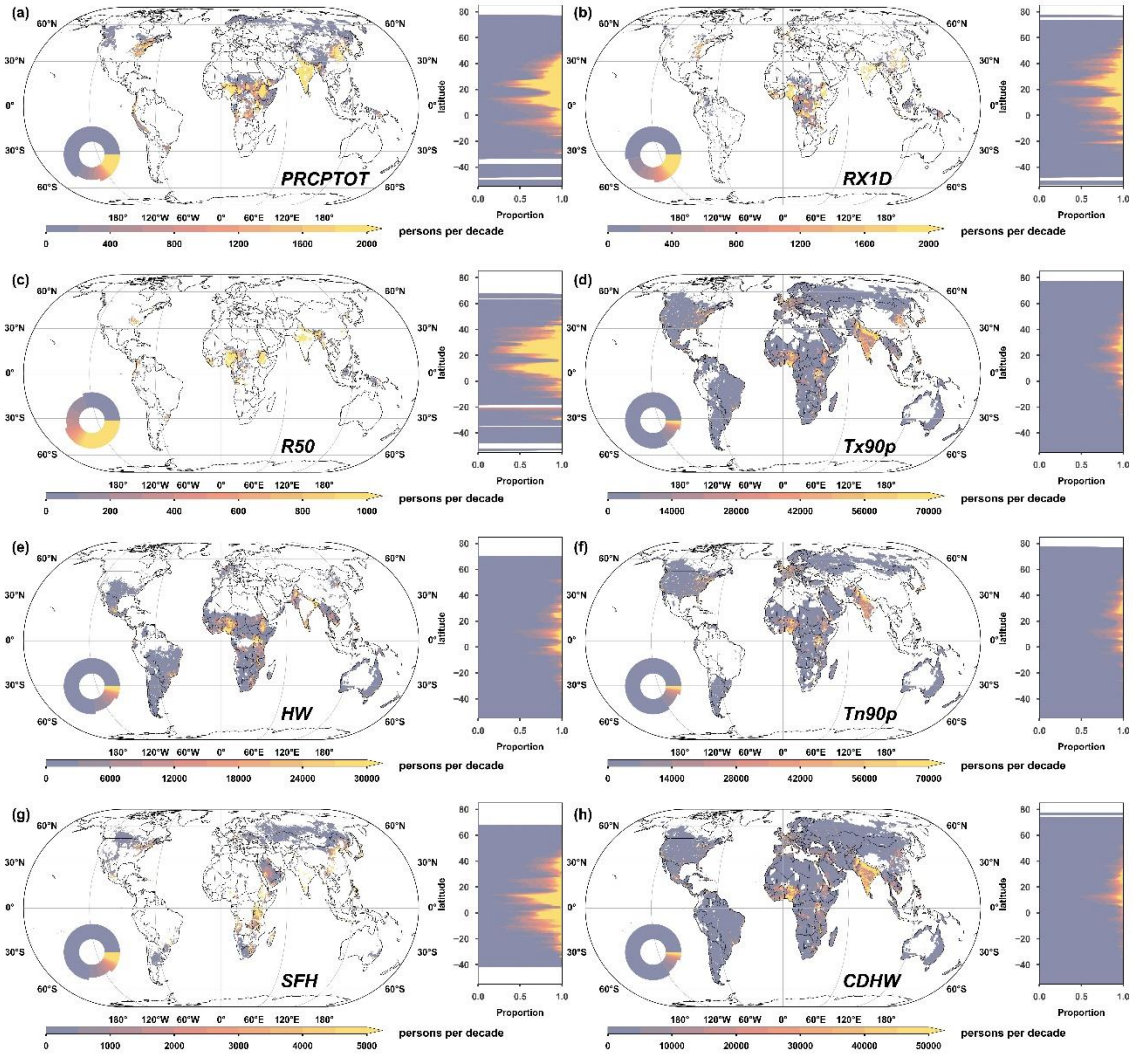

Figure S19. Multimodel median EAE growth rates for different climate extreme indices projected under the SSP5-8.5 scenario from the 2020s to 2090s: (a) PRCPTOT, (b) RX1D, (c) R50, (d) Tx90p, (e) HW, (f) Tn90p, (g) SFH, and (h) CDHW.

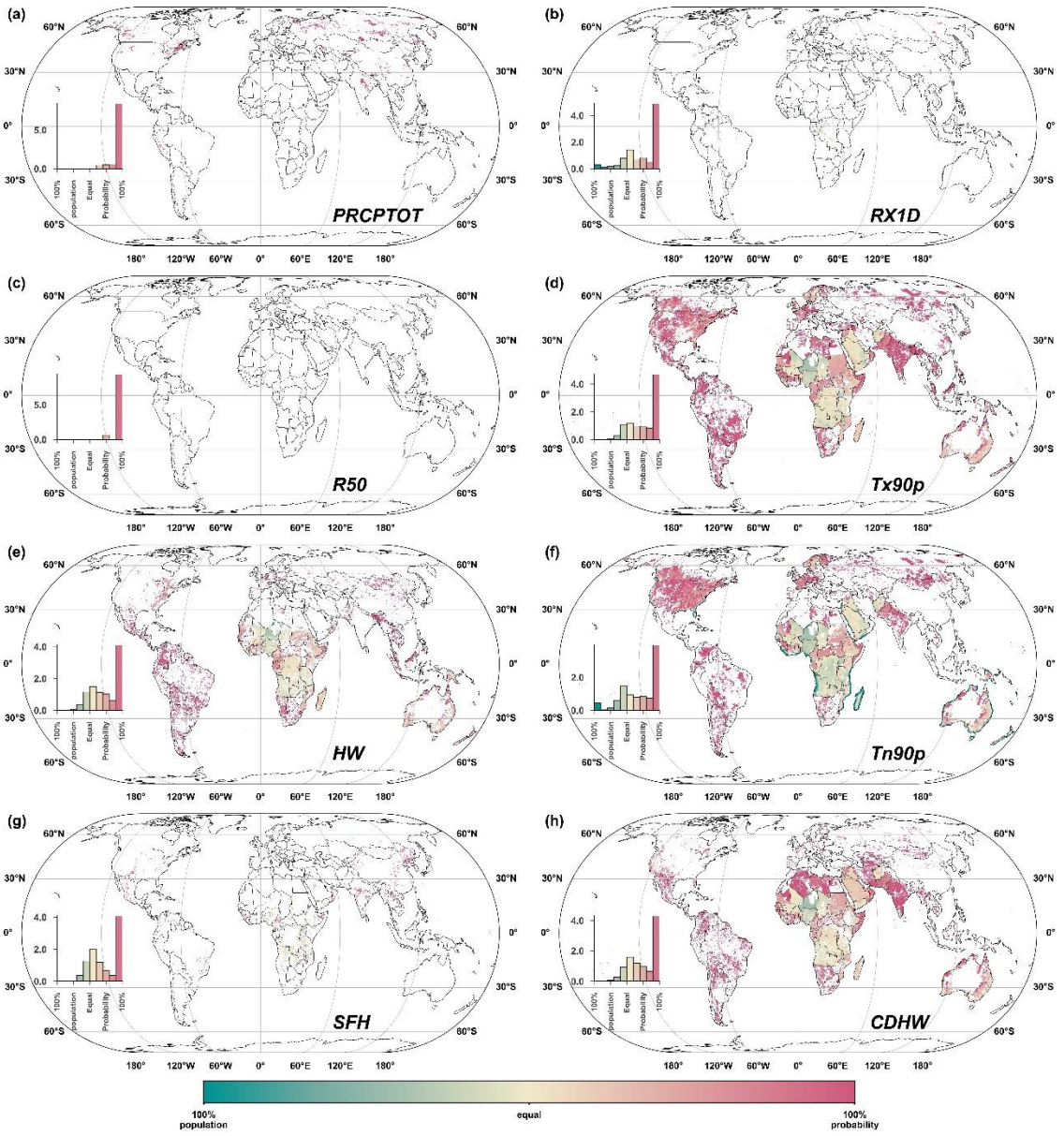

Figure S20. Contributions of record-breaking probability growth and population growth to the multimodel median EAE growth rates for different climate extreme indices projected under the SSP1-2.6 scenario: (a) PRCPTOT, (b) RX1D, (c) R50, (d) Tx90p, (e) HW, (f) Tn90p, (g) SFH, and (h) CDHW. The histograms depict the probability densities at different contribution levels.

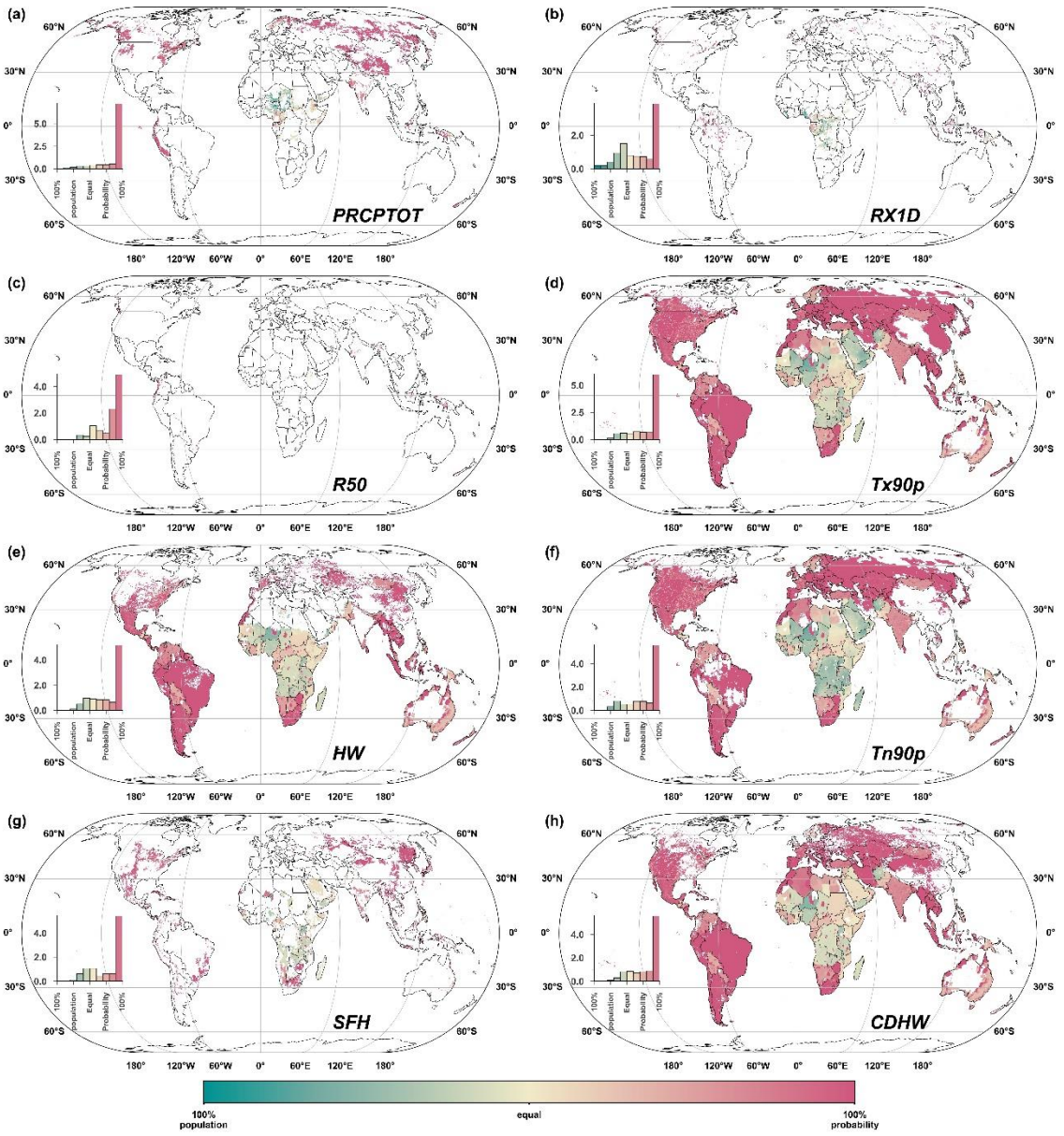

Figure S21. Contributions of record-breaking probability growth and population growth to the multimodel median EAE growth rates for different climate extreme indices projected under the SSP2-4.5 scenario: (a) PRCPTOT, (b) RX1D, (c) R50, (d) Tx90p, (e) HW, (f) Tn90p, (g) SFH, and (h) CDHW. The histograms depict the probability densities at different contribution levels.

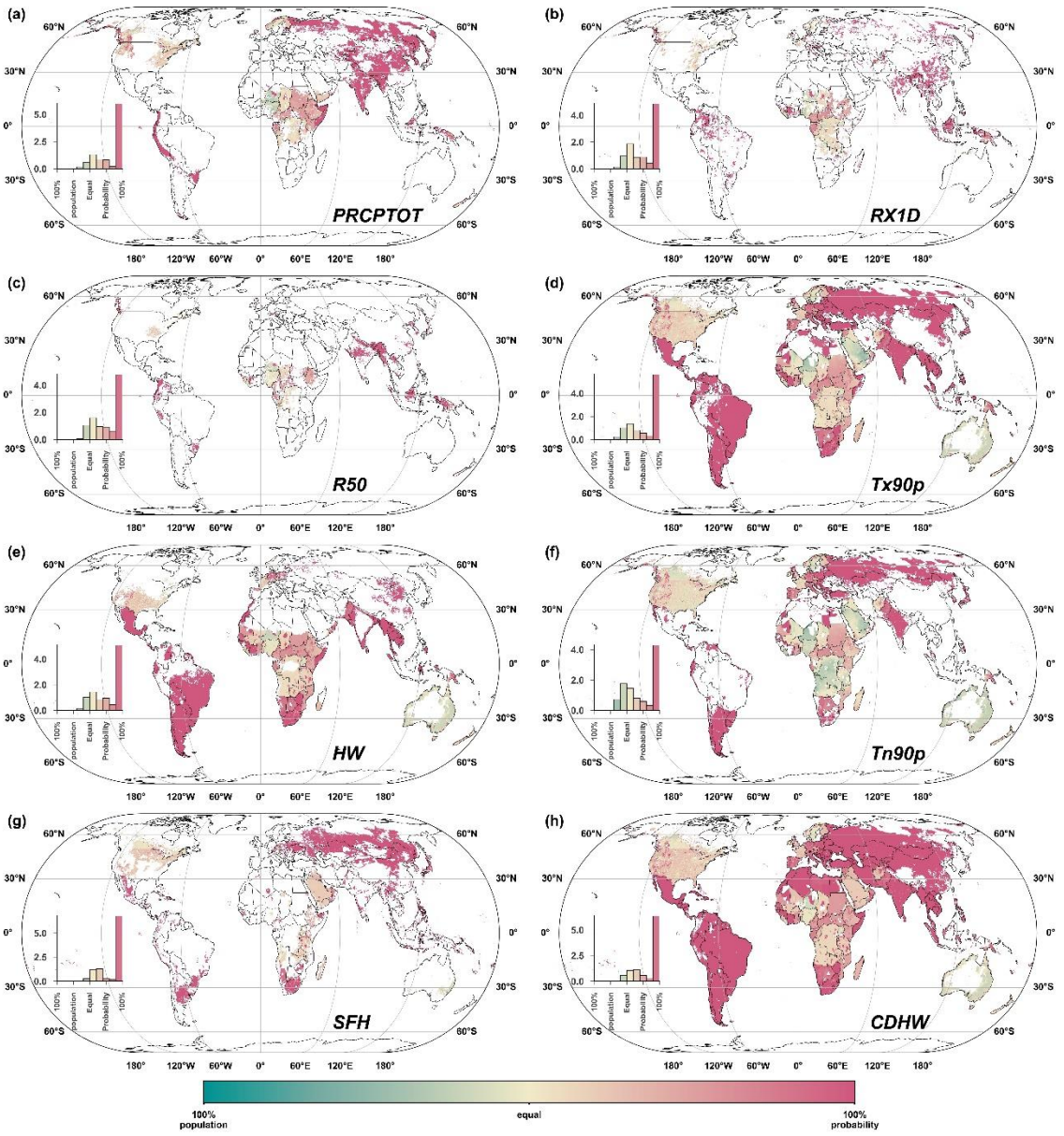

Figure S22. Contributions of record-breaking probability growth and population growth to the multimodel median EAE growth rates for different climate extreme indices projected under the SSP5-8.5 scenario: (a) PRCPTOT, (b) RX1D, (c) R50, (d) Tx90p, (e) HW, (f) Tn90p, (g) SFH, and (h) CDHW. The histograms depict the probability densities at different contribution levels.

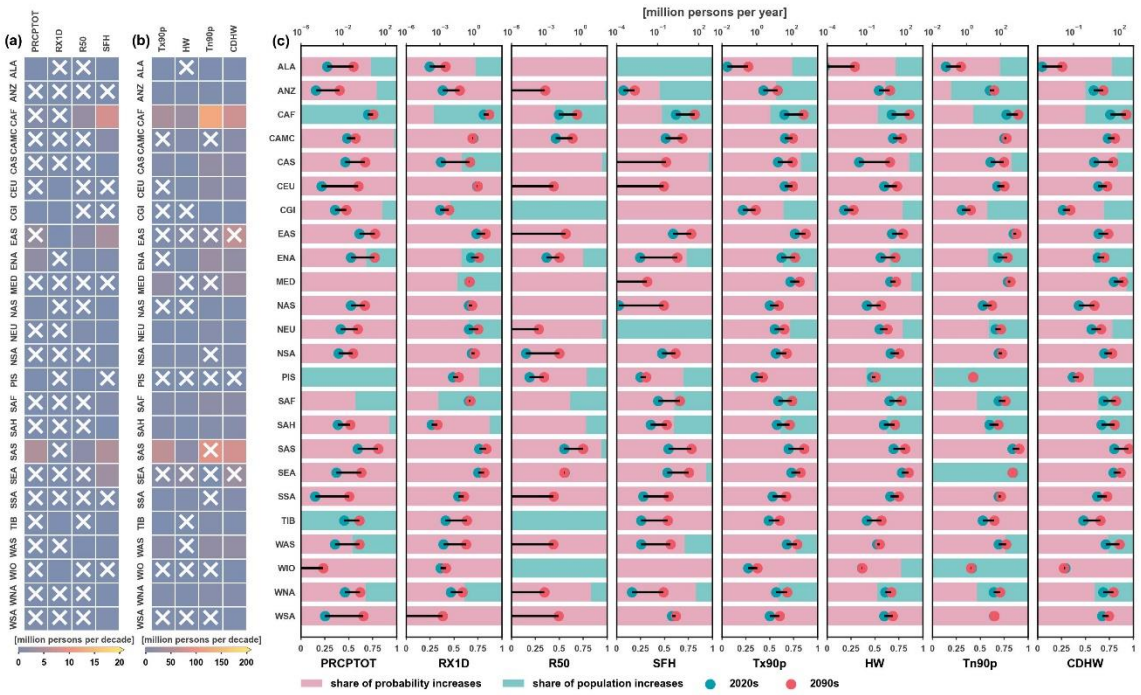

Figure S23. Subcontinental multimodel median EAE variations under the SSP1-2.6 scenario for different climate extreme indices from the 2020s to 2090s: (a) EAE growth rates of PRCPTOT, RX1D, R50, and SFH, (b) EAE growth rates of Tx90p, HW, Tn90p, and CDHW, and (c) Shares of population growth and record-breaking probability growth contributing to the EAE increase in the 2020s and 2090s. The "×" symbols in panels (a) and (b) denote nonsignificant EAE growth (p value <0.05).

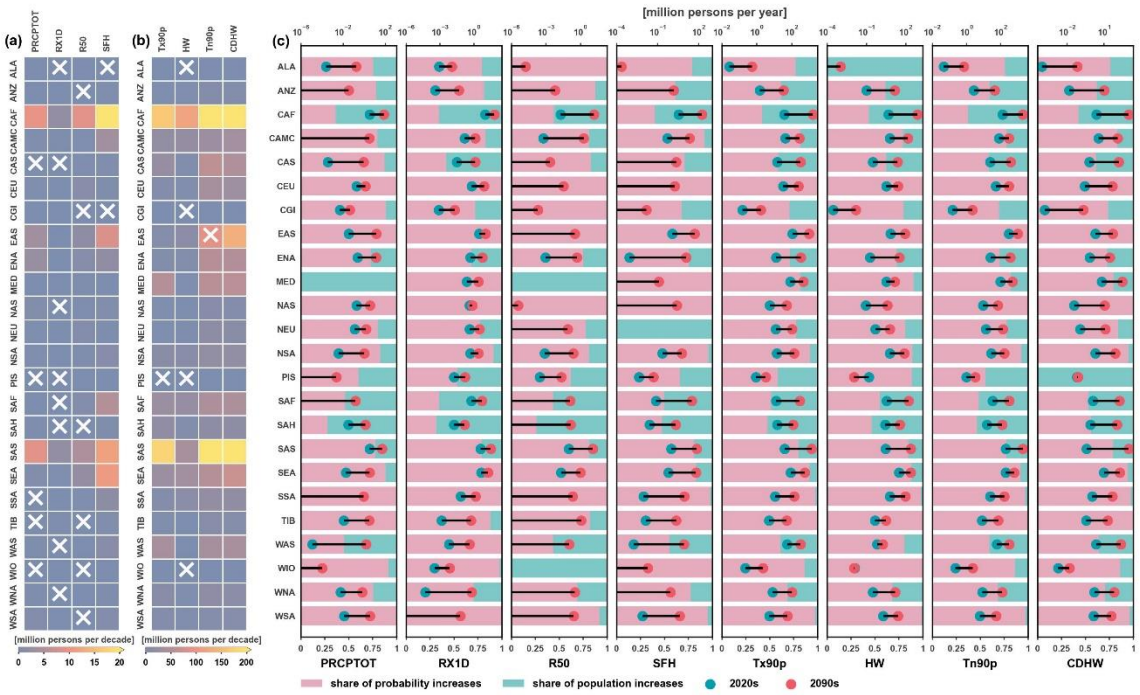

Figure S24. Subcontinental multimodel median EAE variations under the SSP2-4.5 scenario for different climate extreme indices from the 2020s to 2090s: (a) EAE growth rates of PRCPTOT, RX1D, R50, and SFH, (b) EAE growth rates of Tx90p, HW, Tn90p, and CDHW, and (c) shares of population growth and record-breaking probability growth contributing to the EAE increase in the 2020s and 2090s.

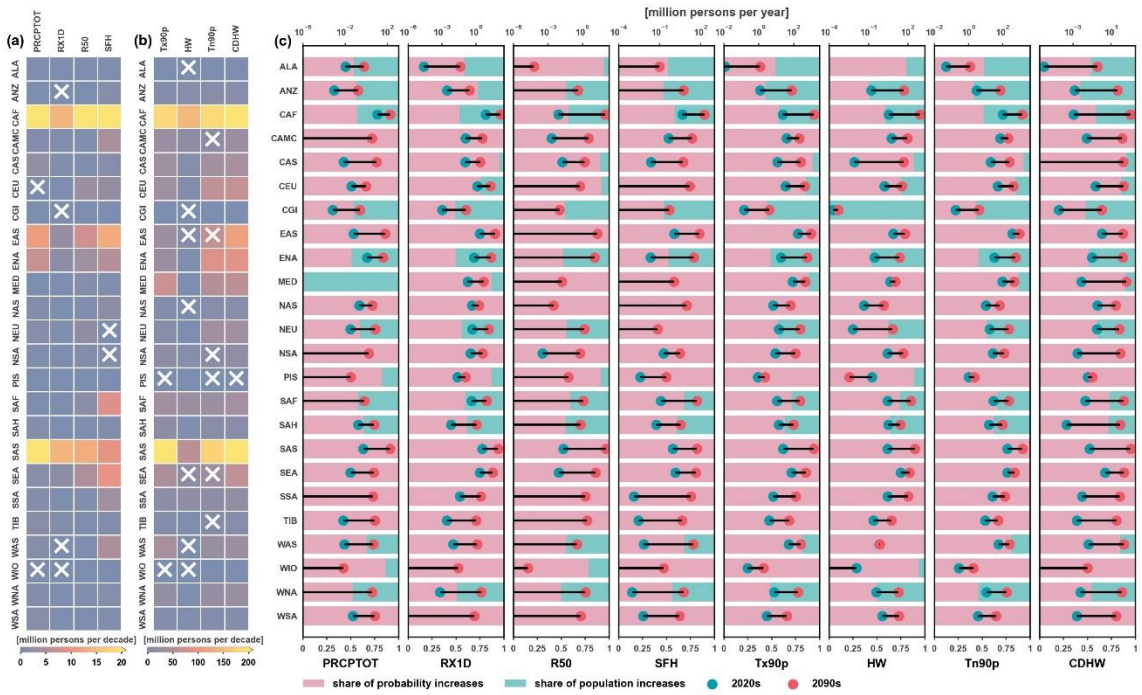

Figure S25. Subcontinental multimodel median EAE variations under the SSP5-8.5 scenario for different climate extreme indices from the 2020s to 2090s: (a) EAE growth rates of PRCPTOT, RX1D, R50, and SFH, (b) EAE growth rates of Tx90p, HW, Tn90p, and CDHW, and (c) shares of population growth and record-breaking probability growth contributing to the EAE increase in the 2020s and 2090s. The "×" symbols in panels (a) and (b) denote nonsignificant EAE growth (p value <0.05).

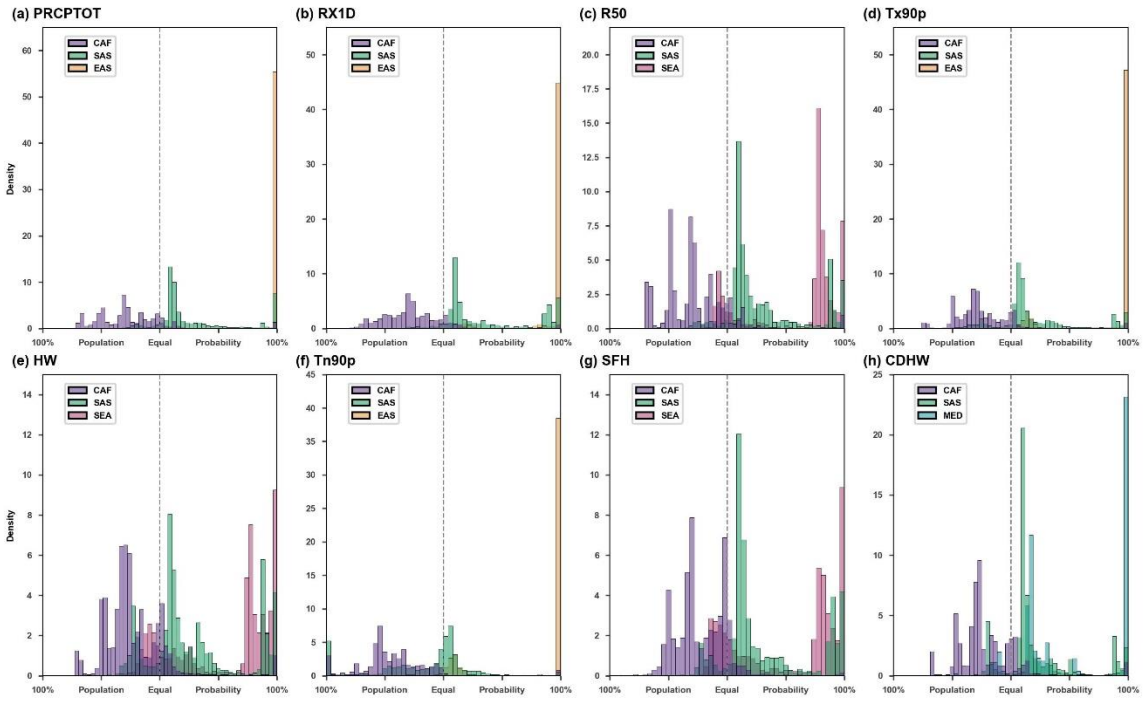

Figure S26. Distributions of the contributions to EAE growth rates in regions with the top three multimodel median EAE growth rates for each climate extreme index under the SSP3-7.0 scenario: (a) PRCPTOT, (b) RX1D, (c) R50, (d) Tx90p, (e) HW, (f) Tn90p, (g) SFH, and (h) CDHW.

Table S1. Summary of the NEX-GDDP-CMIP6 data used in this study. Note: The units of hurs, pr, tas, tasmax, and tasmin are %, kg m-2 s-1, K, K, and K, respectively.

GCM	Institute ID	Variant	Variables	Spatial resolution
ACCESS-CM2	CSIRO-ARCCSS	r1i1p1f1	hurs, pr, tas, tasmax, tasmin	0.25°×0.25°
ACCESS-CM1-5	CSIRO	r1i1p1f1	hurs, pr, tas, tasmax, tasmin	0.25°×0.25°
CanESM5	CCCma	r1i1p1f1	hurs, pr, tas, tasmax, tasmin	0.25°×0.25°
CMCC-ESM2	CMCC	r1i1p1f1	hurs, pr, tas, tasmax, tasmin	0.25°×0.25°
CNRM-CM6-1	CNRM-CERFACS	r1i1p1f2	hurs, pr, tas, tasmax, tasmin	0.25°×0.25°
CNRM-ESM2-1	CNRM-CERFACS	r1i1p1f2	hurs, pr, tas, tasmax, tasmin	0.25°×0.25°
EC-Earth3	EC-Earth-Consortium	r1i1p1f1	hurs, pr, tas, tasmax, tasmin	0.25°×0.25°
EC-Earth3-Veg-LR	EC-Earth-Consortium	r1i1p1f1	hurs, pr, tas, tasmax, tasmin	0.25°×0.25°
GFDL-ESM4	NOAA-GFDL	r1i1p1f1	hurs, pr, tas, tasmax, tasmin	0.25°×0.25°
GISS-E2-1-G	NASA-GISS	r1i1p1f2	hurs, pr, tas, tasmax, tasmin	0.25°×0.25°
INM-CM4-8	INM	r1i1p1f1	hurs, pr, tas, tasmax, tasmin	0.25°×0.25°
INM-CM5-0	INM	r1i1p1f1	hurs, pr, tas, tasmax, tasmin	0.25°×0.25°
IPSL-CM6A-LR	IPSL	r1i1p1f1	hurs, pr, tas, tasmax, tasmin	0.25°×0.25°
KACE-1-0-G	NIMS-KMA	r1i1p1f1	hurs, pr, tas, tasmax, tasmin	0.25°×0.25°
MIROC6	MIROC	r1i1p1f1	hurs, pr, tas, tasmax, tasmin	0.25°×0.25°
MIROC-ES2L	MIROC	r1i1p1f2	hurs, pr, tas, tasmax, tasmin	0.25°×0.25°
MPI-ESM1-2-HR	DKRZ/DWD	r1i1p1f1	hurs, pr, tas, tasmax, tasmin	0.25°×0.25°
MPI-ESM1-2-LR	DKRZ/MPI-M	r1i1p1f1	hurs, pr, tas, tasmax, tasmin	0.25°×0.25°
MRI-ESM2-0	MRI	r1i1p1f1	hurs, pr, tas, tasmax, tasmin	0.25°×0.25°
NorESM2-LM	NCC	r1i1p1f1	hurs, pr, tas, tasmax, tasmin	0.25°×0.25°
NorESM2-MM	NCC	r1i1p1f1	hurs, pr, tas, tasmax, tasmin	0.25°×0.25°
UKESM1-0-LL	MOHC/NIMS-KMA	r1i1p1f2	hurs, pr, tas, tasmax, tasmin	0.25°×0.25°

Table S2. Global EAE differences among scenarios in the late-21st century.

	SSP1-2.6	SSP2-4.5	SSP3-7.0	SSP5-8.5	SSP3-7.0/SSP1-2.6	SSP3-7.0/SSP2-4.5	SSP3-7.0/SSP5-8.5
PRCPTOT	192258875	3.29E+08	7.65E+08	5.47E+08	3.980597	2.324469	1.398486
RX1D	168492367	3.03E+08	6.45E+08	4.66E+08	3.82751	2.12987	1.382641
R50	48090887	1.31E+08	4E+08	2.99E+08	8.327843	3.049114	1.340421
Tx90p	3.123E+09	7.16E+09	1.14E+10	7.23E+09	3.649899	1.591176	1.577254
HW	812676688	2.03E+09	4E+09	2.03E+09	4.920138	1.969438	1.971175
Tn90p	5.363E+09	8.72E+09	1.26E+10	7.37E+09	2.353592	1.446928	1.713328
SFH	187447441	5.02E+08	1.02E+09	5.69E+08	5.438645	2.032117	1.793208
CDHW	1.469E+09	3.72E+09	7.75E+09	4.4E+09	5.27489	2.081912	1.761066

Note: Columns with yellow headings represent the total global EAE (unit: persons per year), and columns with blue headings refer to the ratio of the total global EAE under different scenarios.

Table S3. Global EAE trend differences among scenarios from the 2020s to the 2090s.

	SSP1-2.6	SSP2-4.5	SSP3-7.0	SSP5-8.5	SSP3-7.0/SSP1-2.6	SSP3-7.0/SSP2-4.5	SSP3-7.0/SSP5-8.5
PRCPTOT	10155308	28061378	96678909	80204577	9.520037	3.445266	1.205404
RX1D	6590453	21626790	65972050	59677203	10.01025	3.050478	1.105482
R50	580158.7	514481 4	347992 73	361854 85	59.98233	6.763952	0.961691
Tx90p	3.91E+08	1.08E+09	1.65E+09	1.13E+09	4.216491	1.526406	1.46027
HW	98313704	3.09E+08	5.71E+08	3.35E+08	5.804647	1.84499	1.702428
Tn90p	3.86E+08	1.12E+09	1.36E+09	8.82E+08	3.515161	1.212485	1.538487
SFH	22120686	74174628	1.47E+08	93736479	6.631342	1.977628	1.564917
CDHW	1.88E+08	6.14E+08	1.19E+09	8.15E+08	6.328319	1.936713	1.458646

Note: Columns with yellow headings represent the total global EAE growth rates (unit: persons per decade), and columns with blue headings refer to the ratio of the total global EAE growth rates under different scenarios.

Table S4. Differences in the contribution of record-breaking probability growth driving global EAE growth under different scenarios.

	SSP1-2.6	SSP2-4.5	SSP3-7.0	SSP5-8.5	SSP1-2.6/SSP3-7.0	SSP2-4.5/SSP3-7.0	SSP5-8.5/SSP3-7.0
PRCPTOT	0.53112047	0.73453693	1.04011763	0.91603067	1.95834597	1.38299495	1.72471355
RX1D	0.55770639	0.70651638	0.93554593	0.88338629	1.67748827	1.26682497	1.58396301
R50	0.48745277	0.67417356	0.90406021	0.86903811	1.85466217	1.38305412	1.782815
Tx90p	0.62300207	0.80489629	1.0640211	0.93371123	1.70789336	1.29196407	1.49872894
HW	0.50641718	0.70048422	0.9782655	0.84715112	1.93173837	1.38321575	1.67283251
Tn90p	0.50888373	0.76829548	1.05459589	0.93190456	2.07237101	1.50976625	1.83127207
SFH	0.55768418	0.73357879	0.96654284	0.93720827	1.73313656	1.31540183	1.68053587
CDHW	0.54101108	0.68817723	0.86211048	0.88159943	1.59351723	1.27202058	1.62954043

Note: Columns with yellow headings represent the contribution of record-breaking probability growth driving global EAE growth, and columns with blue headings refer to the ratio of contributions under different scenarios